LIMNOLOGY and OCEANOGRAPHY

ASLO

Limnol. Oceanogr. 68, 2023, 1936–1948

doi: 10.1002/lno.12396

Low carbon accumulation in a macro-tidal mangrove forest on the Amazon coast

Tiago Passos,[1*] **Angelo F. Bernardino**,[2] **Dan Penny**,[1] **Roberto Barcellos**,[3] **Francisco U. Passos**,[4] **Gabriel N. Nobrega**,[5] **Tiago O. Ferreira**,[6] **J. Boone Kauffman**,[7] **Christian J. Sanders**[8]

[1]The University of Sydney, School of Geosciences, Camperdown, New South Wales, Australia
[2]Department of Oceanography, Federal University of Espírito Santo, Vitória, Espírito Santo, Brazil
[3]Department of Oceanography, Federal University of Pernambuco, Recife, Pernambuco, Brazil
[4]SENAI CIMATEC Technology College, Salvador, Bahia, Brazil
[5]Department of Soil Sciences, Federal University of Ceará, Fortaleza, Ceará, Brazil
[6]Department of Soil Sciences, Luiz de Queiroz College of Agriculture, University of Sao Paulo, Piracicaba, São Paulo, Brazil
[7]Department of Fisheries, Wildlife, and Conservation Sciences, Oregon State University, Corvallis, Oregon, USA
[8]National Marine Science Centre, Southern Cross University, Coffs Harbour, New South Wales, Australia

Abstract

The important role mangrove forests play in sequestering organic carbon is well known, yet rates of organic carbon accumulation in macro-tidal mangrove ecosystems are poorly resolved. Here we use ^{210}Pb dating to present a 125-yr record of carbon, nutrient and trace metal accumulation in sediments from an Amazon macro-tidal mangrove forest. We find that the rate of organic carbon accumulation ranged from 23.7 to 74.7 g m^{-2} yr^{-1} (average 38 ± 13.5 g m^{-2} yr^{-1}), significantly lower than global averages for mangrove forests. These low rates may be associated with sediment grain-size and sediment–water interface processes that drive organic matter oxidation and reduce carbon stocks in these highly dynamic macro-tidal forests. Total nitrogen accumulation ranged from 1.4 to 5.1 g m^{-2} yr^{-1} (average 2.7 ± 0.9 g m^{-2} yr^{-1}) and phosphorus from 1.5 to 8.4 g m^{-2} yr^{-1}(average 4.3 ± 1.9 g m^{-2} yr^{-1}). Trace metal accumulation rates (As, Pb, Cr, Cu, Mn, Ni, Zn, Hg, Bo, V, Co, Mo, S, and Ba) were also lower than other tropical mangrove forests globally, but trace metal in more recent sediments for Mn, As, Cu, and Hg were elevated, likely reflecting human footprint in the region since early the 20th century. The ability to accurately quantify carbon accumulation rates in mangrove ecosystems is critical for climate change mitigation strategies and the implementation of carbon offset schemes globally.

*Correspondence: tiago.passos@sydney.edu.au

Additional Supporting Information may be found in the online version of this article.

Author Contribution Statement: T.P.: Conceptualization (lead); writing—original draft (lead); investigation; formal analysis (lead—grain-size, ^{210}Pb, trace metals, carbon and nitrogen); interpretation of data; writing, review and editing. A.F.B.: Conceptualization (supporting); funding acquisition; data collection; supervision; interpretation of data; review and editing. D.P.: Supervision, review and editing. R.B.: Supervision, review and editing. F.U.P.: Investigation, review and editing. G.N.B.: Data collection, review and editing. T.O.F.: Data collection, review and editing. J.B.K.: Data collection, review and editing. C.J.S.: Conceptualization (supporting), data collection, formal analysis (supporting—grain-size, ^{210}Pb, trace metals, carbon and nitrogen); interpretation of data; supervision; review and editing.

The term "blue carbon" was coined over a decade ago to describe the significant contribution coastal wetlands (e.g., mangroves, seagrasses, and saltmarshes) make to global carbon sequestration (Mcleod et al. 2011). Mangrove forests are diverse ecosystems with the capacity to produce and store large amounts of organic carbon at higher rates per unit area than terrestrial forests (Alongi 2014; Kauffman et al. 2020). The capacity of mangrove forests to sequester organic carbon during sediment burial is considered a critical ecological service in the carbon cycle (Sanders et al. 2010; Alongi 2014), and plays a key role in mitigating global climate change (Wang et al. 2021; Passos et al. 2022). In addition, mangrove forests can store nutrients, trace metals and other pollutants from terrestrial sources that can impact marine ecosystems when discharged in coastal areas (Kristensen et al. 2008).

Organic carbon accumulation in tidal wetlands is controlled by nutrient availability (Sanders et al. 2014), source of organic matter (Sanders et al. 2010), climatic factors

(e.g., rainfall and temperature) (Lovelock et al. 2014; Kauffman et al. 2020), and oceanographic processes (e.g., currents, morphology, and tidal amplitude) (Wang et al. 2021). Land use changes may trigger rapid changes in organic carbon in addition to losses of ecosystem carbon stocks (Bernardino et al. 2020). The effects of land use over mangrove can also trigger an increase in sediment loads and nutrient fluxes to nearby estuaries, which can lead to eutrophication (Borges et al. 2009; Pérez et al. 2018; Passos et al. 2021*a*) and geochemical implications in blue carbon environments (Sippo et al. 2020; Passos et al. 2022).

The conversion of mangroves to shrimp farms is a major source of disturbance in mangroves globally. In addition to the immediate removal of ecosystem carbon stocks (Kauffman et al. 2018*a*; Pérez et al. 2020; Passos et al. 2022), shrimp farms lead to shifts in inorganic supply nearby mangroves from terrigenous to aquatic (i.e., algal-derived) sources of organic matter, which can impact carbon accumulation rates. The organic carbon accumulation efficiency of algae-derived sources of organic matter is estimated to be considerably smaller ($\sim$ 0.1%) than seagrasses, mangrove forests and terrestrial vascular plants (up to 10%) (Mcleod et al. 2011; Macreadie et al. 2012), so the shift toward such source can have the net effect of reducing carbon sequestration in degraded mangrove ecosystems (Sanders et al. 2010; Macreadie et al. 2019). In addition, the discharge of nutrient-rich effluents in mangrove soils triggers organic matter decomposition rates resulting in lower organic carbon stocks (Nóbrega et al. 2016; Nóbrega et al. 2019). Identifying the elements controlling organic carbon accumulation rates is critical for understanding the fate of the carbon buried in tidal wetlands, particularly under global climate change scenarios, including sea-level rise (Lovelock et al. 2015; Rogers et al. 2019). Furthermore, quantifying organic carbon accumulation in mangrove forests with distinct geomorphology and tidal regimes may serve as a basis for restoration programs, indicating natural rates for carbon sequestration.

Here, we use dated sediment cores from a highly dynamic macro-tidal Amazon mangrove forest to resolve historical trends in carbon, nutrient, and trace metal accumulation rates. We build on the blue carbon environmental literature by (1) constraining the relative contribution of organic carbon, nutrient and trace metals accumulation rates in a tropical macro-tidal estuary; (2) assessing potential biogeochemical dissimilarities between impacted and pristine mangroves; (3) providing a robust set of data that enables environmental monitoring and rehabilitation of biodiverse tropical mangroves threated by deforestation; and (4) contributing to global estimates of carbon, nutrient and trace metals retention in blue carbon environments. We tested the hypothesis that sediments in tropical macro-tidal mangrove forests preserve organic carbon, nutrient, and trace metal accumulation at high rates.

Material and methods

Study site

The study site is located in the tropical Mocajuba and Curuçá estuarine systems (00°41′ to 00°45″S and 47°51′ to 47°57′W), Pará state, on the Brazilian Amazon coast (Fig. 1). The sampling locations were strategically chosen to compare stratigraphic records between mangrove forests near shrimp ponds (cores 1 and 2) and pristine mangrove forests (cores 3 and 4). All sites, including the Mocajuba and Curuçá estuaries, are located in the east margin of the Amazon Delta and are part of a complex estuarine system with a macro-tidal regime. The semidiurnal tides have amplitudes ranging from 3.5 m during neap tide to over 6 m during spring tide (Matos et al. 2020), with tidal currents range from 1.9 to 2.1 knots (0.97–1.08 m s^{-1}) (Mourão et al. 2020). The climate in this region is tropical monsoonal (Am), according to Köppen-Geiger classification (Matos et al. 2020), with an annual average temperature of $\sim$ 27°C, with a small seasonal variation and average rainfall of 2500 mm yr^{-1} (Bernardino et al. 2015).

The geological setting is mostly composed of fine to medium siliciclastic sandstones from the Tertiary Barreiras Formation, forming the tablelands with elevations varying from 20 to 100 m (Rossetti et al. 2013). In the lowers areas of the coastal plain, Holocene-age sediments are predominant. The basement of the coastal plain is composed by igneous and metamorphic Proterozoic formations (Rossetti et al. 2013).

The main rivers discharging to this part of the Amazon estuarine system are the Mocajuba and Curuçá, including the Furo Maripanema creek connecting them. Riverine and soil salinity are typically euryhaline, which is markedly distinct from mangrove sites to the West in the Amazon Delta (Kauffman et al. 2018*b*; Bernardino et al. 2022). The Mocajuba river, located $\sim$ 225 km east of the Amazon River mouth, has 323 km^2 of catchment area, 53 km of estuarine length, 54.5 km^2 of mangrove forests and 11 m s^{-1} of river discharge (Gomes et al. 2021). The Curuçá estuary area is $\sim$ 200 km^2, and it is covered by $\sim$ 116 km^2 of mangrove forests, dominated by *Rhizophora mangle* L., *Laguncularia racemosa* (L.) C.F.Gaertn., and *Avicennia germinans* (L.) L. (Kauffman et al. 2018*b*; Matos et al. 2020). The mangrove trees in the region are tall (up to 35 m), and saltmarsh vegetation is often located along the upper tidal regions, dominated by a variety of graminoid species, including *Spartina brasiliensis* Radd, *Schoenoplectus* sp., and *Distichlis* sp. (Kauffman et al. 2018*b*; Matos et al. 2020).

Shrimp ponds were established in the Curuçá estuary (Fig. 1) in the 1980s but is limited regionally due to the permanent protection status of mangroves (Bernardino et al. 2021). Shrimp farms produce white leg shrimp (*Litopenaeus vannamei* (Boone, L. 1931)), with the harvest occurring in up to three cycles per year and the production mostly exported to Europe.

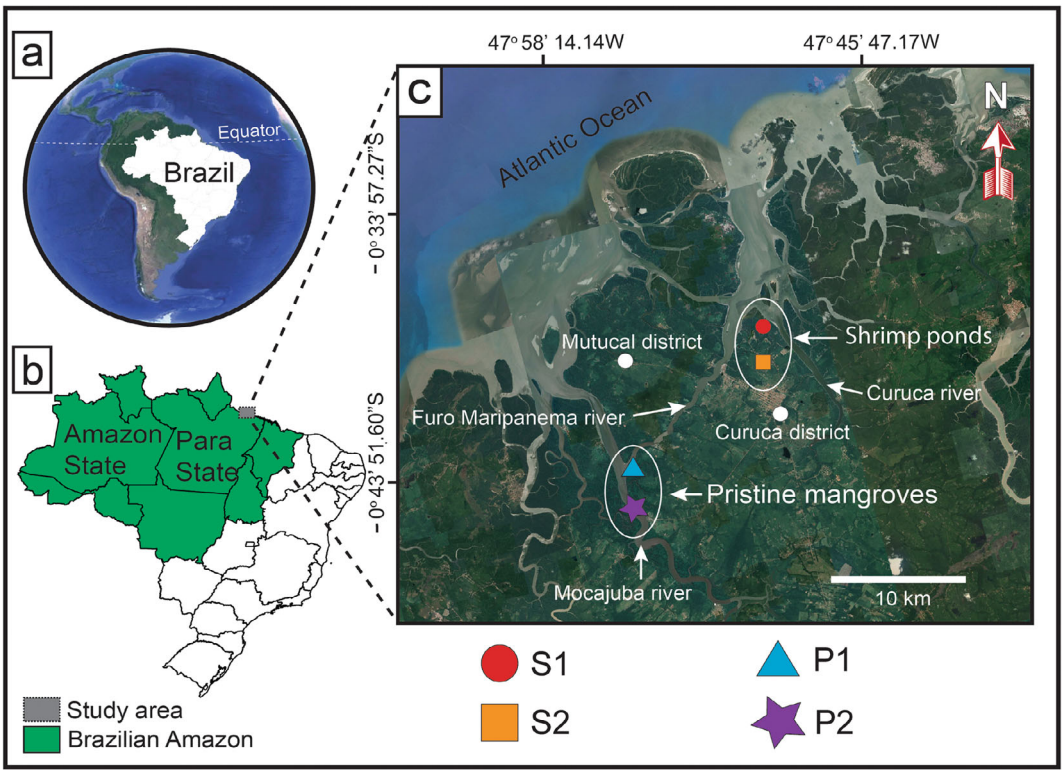

Fig. 1. Study site location. (**a**) Brazil; (**b**) Brazilian Amazon including the Pará state where the sites are located; (**c**) location of sediment core sampling near shrimp ponds (S1 and S2) and in a pristine area (P1 and P2).

Sediment sampling and analyses

Four sediment cores were collected in 2019 from mangrove forests adjacent to the Curuçá and Mocajuba rivers (Fig. 1), using a Russian sediment borer and a 60 mm diameter polyvinyl chloride tube (no compaction was observed during collection). The Curuçá river sampling sites were located in mangrove forests near shrimp ponds (S1 and S2) and therefore were potentially under the influence of the effluents from these sites (Nóbrega et al. 2013). The sediment cores were subsampled in 2 cm intervals from the top of the core to 10 cm depth, and then at 5 cm intervals down core to the base, maximum of 45 cm depth, until refusal. Each subsample was analyzed for dry bulk density, grain-size distribution, organic carbon, total nitrogen, total phosphorus, total sulfur, nitrogen and carbon stable isotope ratios ($\delta^{15}N$ and $\delta^{13}C$, respectively) and total content of trace metals (As, Pb, Cr, Cu, Mn, Ni, Zn, Hg, Bo, V, Co, Mo, and Ba). Sediment accretion rates and sediment ages were obtained through the ^{210}Pb and ^{226}Ra analysis.

Pretreatment for grain-size analysis involved oxidization of organic matter with 30% wt/vol H_2O_2 and deflocculation of mineral clasts with 5% $Na_6[(PO_3)_6]$ (Sperazza et al. 2004). Grain-size distribution was measured by a Malvern Mastersizer 3000 laser diffractometer with a wet dispersion unit. Laser diffractometer can measure very fine-grained sediments (< 10 μm) efficiently, with high precision (~ 5% at 2 standard deviations), and without the need for extensive mineralogical determinations (Sperazza et al. 2004). Dry bulk density was determined by drying sediment subsamples in an oven for 72 h at 60°C, with the resulting dry mass of each subsample divided by its volume (g cm^{-3}) (Ravichandran et al. 1995). Organic carbon, stable carbon isotopic ratio ($\delta^{13}C$), total nitrogen, and stable nitrogen isotopic ratio ($\delta^{15}N$) were determined for each depth interval using ~ 20 mg of dried and homogenized sediment packed into tin pellets (Passos et al. 2022). A Thermo Finnigan Model Delta Plus XP with analytical precision of N = 0.1%, was used to measure organic carbon, total nitrogen, ($\delta^{13}C$), and ($\delta^{15}N$), following the procedure described by Naidu et al. (2000). Samples in silver pellets were treated with 37% wt/vol HCl to remove inorganic carbon ($CaCO_3$), intended for organic carbon and $\delta^{13}C$ analysis. The total phosphorus for each depth interval were determined by total digestion procedures followed by the colorimetric method using a HITACHI model U-1100 spectrometer.

Trace metal content was determined using a Perkin Elmer NexION 350D ICPMS using total digestion procedures described by Passos et al. (2022). Enrichment factors were determined using aluminum to normalize geochemical data (Miola et al. 2016). Aluminum is used to normalize the data as it is a stable lithogenic element that is redox-stable in mangrove environments, and less likely to be affected by anthropogenic sources (Xavier et al. 2017). Enrichment factors up to

1 indicates natural lithogenic fluctuations, while enrichment factors > 1.5 indicate anthropogenic influence (Zhang and Liu 2002; Conrad et al. 2017; Passos et al. 2021*b*).

Radionuclide analyses were conducted to determine the age of the sediment and calculate sediment accretion rates. Homogenized sediment samples (~ 5 g) were packed and sealed with epoxy resin in polypropylene vials, were left for at least 21 d to allow ^{222}Rn to establish secular equilibrium between ^{226}Ra and its granddaughter ^{214}Pb (Conrad et al. 2017). The samples were counted in a high purity germanium (HPGe) detector. The ^{210}Pb activity was determined using the 46.5 keV gamma peak (Sanders et al. 2010; Passos et al. 2022), and ^{226}Ra activity was determined by averaging peaks from its daughters ^{214}Bi and ^{214}Pb (295.2, 351.9, and 609.3 keV) (Moore 1984). Excess ^{210}Pb was determined by deducting ^{226}Ra from the total ^{210}Pb activity (Cutshall et al. 1983). The ^{210}Pb excess was used to determine sediment accretion rates following the Constant Initial Concentration model (Appleby and Oldfield 1992). Then, the sediment

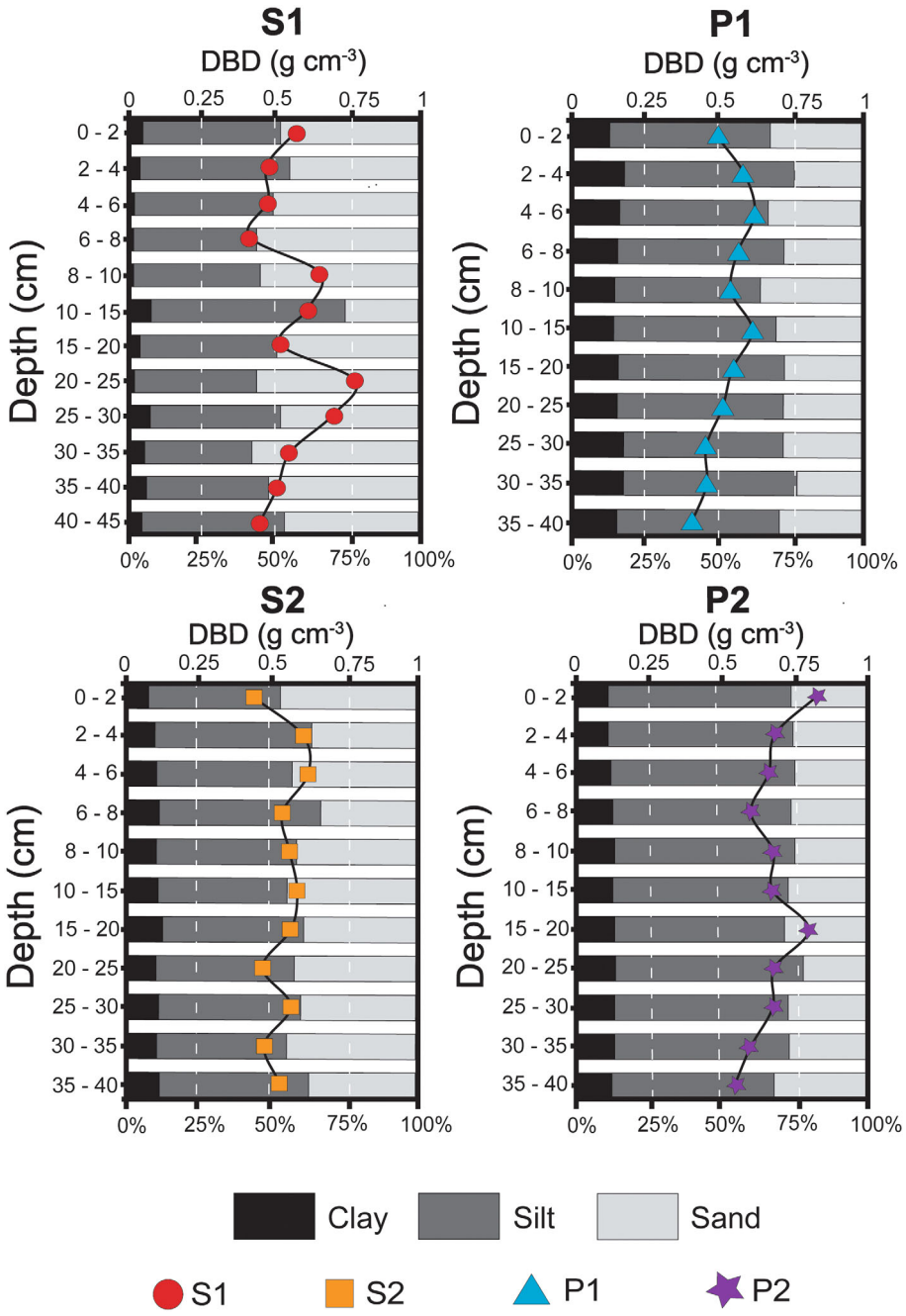

Fig. 2. Vertical distribution of grain-size (bars) and dry bulk density (DBD) (dots, squares, triangles, and stars) for all cores.

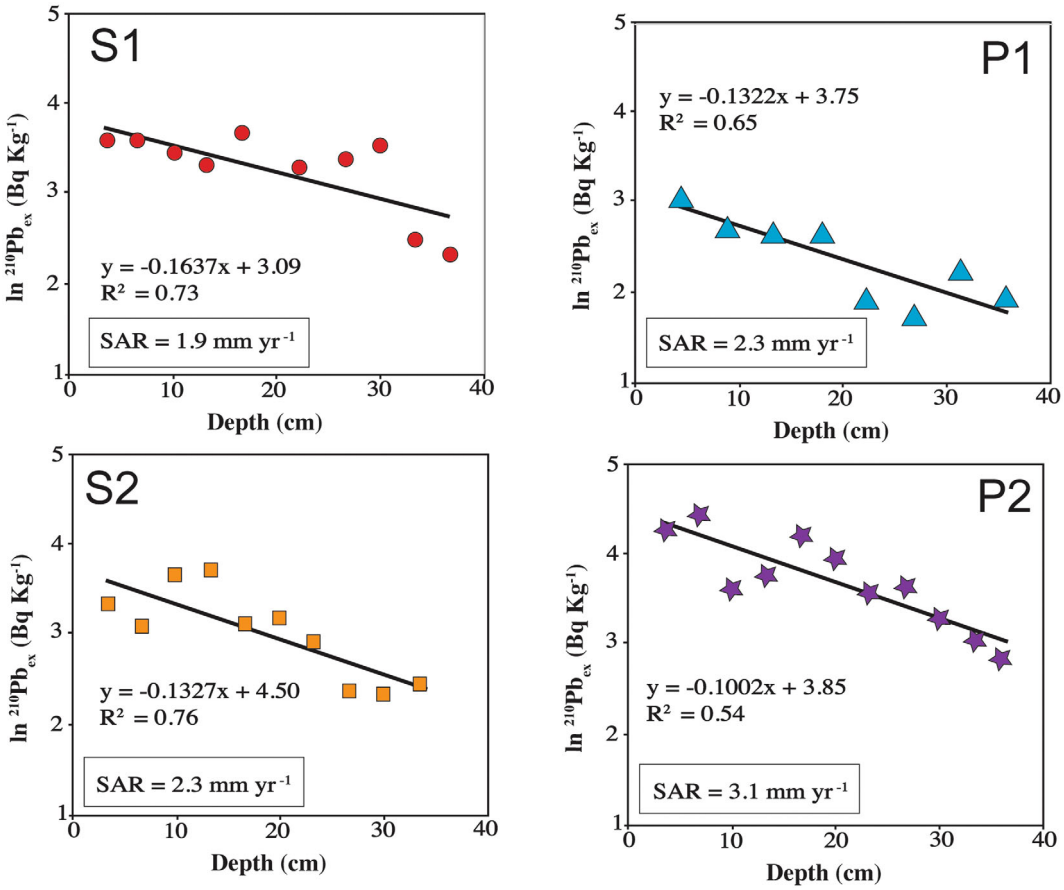

Fig. 3. Excess ^{210}Pb profiles from S1, S2, P1, and P2 in Amazon coast, Brazil. Sediment accretion rates (SAR) are calculated using the Constant Initial Concentration method (Appleby and Oldfield 1992).

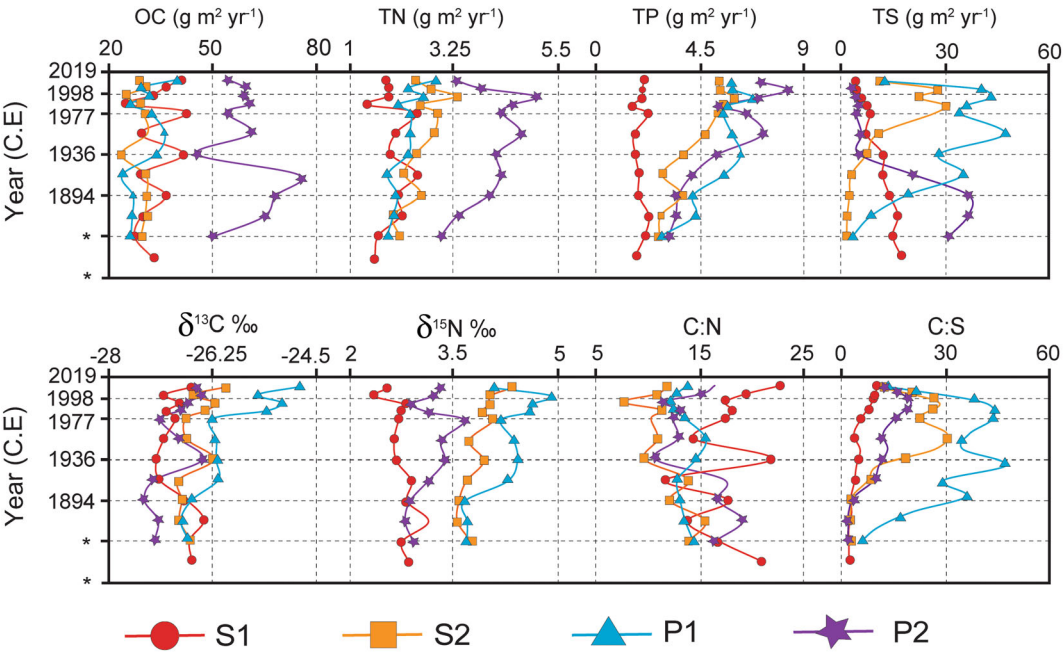

Fig. 4. (**a**) Vertical profiles of accumulation rates (g m^{-2} yr^{-1}) of organic carbon (OC), total nitrogen (TN), total phosphorus (TP), and total sulfur (TS) for S1, S2, P1, and P2. (**b**) Stable carbon isotope (δ^{13}C), stable nitrogen isotope (δ^{15}N), C : N, and C : S ratios for S1, S2, P1, and P2.

Table 1. Minimum, maximum, mean values and standard deviation (SD) of total organic carbon (TOC), total nitrogen (TN), total phosphorus (TP), total sulfur (TS), C : N molar ratios and $\delta^{13}C$ and $\delta^{15}N$ for sediment S1, S2, P1, and P2.

Variable		S1	S2	P1	P2
TOC (%)	Min	1.98	1.77	1.54	2.71
	Max	4.26	2.93	2.37	4.90
	Mean	3.27	2.40	1.98	3.71
	SD	0.69	0.38	0.23	0.76
TOC (g m^{-2} yr^{-1})	Min	25.04	23.76	23.75	45.45
	Max	42.83	31.13	40.01	74.72
	Mean	33.61	29.01	30.18	59.08
	SD	5.96	2.43	5.01	8.32
TN (%)	Min	0.16	0.17	0.12	0.21
	Max	0.21	0.25	0.17	0.29
	Mean	0.18	0.21	0.15	0.25
	SD	0.02	0.02	0.01	0.02
TN (g m^{-2} yr^{-1})	Min	1.37	1.95	1.82	2.98
	Max	2.47	3.30	2.88	5.06
	Mean	1.91	2.54	2.21	4.06
	SD	0.33	0.39	0.42	0.64
TP (%)	Min	126.24	229.11	229.11	247.81
	Max	224.43	542.38	458.22	467.57
	Mean	186.25	358.33	349.83	338.35
	SD	34.75	98.08	64.85	80.34
TP (g m^{-2} yr^{-1})	Min	1.56	2.73	2.79	3.14
	Max	2.29	6.01	6.85	8.37
	Mean	1.91	4.39	5.36	5.59
	SD	0.24	1.24	1.15	1.81
TS (%)	Min	0.37	0.08	0.04	0.16
	Max	2.07	2.93	0.71	2.65
	Mean	1.01	0.60	0.14	1.00
	SD	0.51	0.66	0.20	1.09
TS (g m^{-2} yr^{-1})	Min	4.06	0.95	0.67	2.98
	Max	17.33	6.01	8.66	36.87
	Mean	10.32	4.39	2.02	14.25
	SD	4.68	7.53	2.40	14.30
C : N	Min	11.77	7.58	12.30	10.81
	Max	22.92	15.63	15.67	19.25
	Mean	17.84	11.71	13.63	14.84
	SD	3.33	2.24	1.01	2.74
C : S	Min	1.80	1.42	3.03	1.57
	Max	10.10	30.30	47.62	19.89
	Mean	4.21	13.06	28.13	9.31
	SD	2.68	11.51	15.14	6.30
$\delta^{13}C$	Min	−27.23	−26.85	−26.82	−27.45
	Max	−26.43	−26.02	−24.77	−26.44
	Mean	−26.87	−26.56	−25.97	−26.94
	SD	0.26	0.28	0.69	0.35
$\delta^{15}N$	Min	2.37	3.54	3.64	2.81
	Max	3.14	4.30	4.87	3.64
	Mean	2.75	3.85	4.20	3.15
	SD	0.19	0.23	0.41	0.25

age was calculated following the equation: [years of sampling] – [average depth of sediment interval]/sediment accretion rates. The ^{210}Pb dating method is the most widely used radionuclide tracer to estimate decade to century age of sediment (Sanders et al. 2016). Sediment deposition can be accurately estimated back to ~ 120 yr depending on analytical uncertainties (Appleby and Oldfield 1992).

The sedimentary organic carbon, total nitrogen, total phosphorus, total sulfur, and trace metal fluxes were estimated using the sediment accretion rates, dry bulk density and the depth for each interval in the core. The fluxes (g m^{-2} yr^{-1}) for each variable were calculated following Sanders et al. (2014).

Results

Sedimentary characteristics and sediment accretion rates

All cores are characterized by fine sediments (e.g., clay + silt; Fig. 2). S1 and S2 show an average of 50.9 ± 8.6% and 59.4 ± 4.2% of silt and clay (< 63 μm) content, respectively. P1 and P2 show a higher silt and clay content, 73.4 ± 2.4% and 71.5.4 ± 3.8%, respectively. In general, the sites near shrimp ponds (S1 and S2) in the Curuçá estuary, are coarser (higher sand content) than the values on the pristine sites (P1 and P2), located in the Mocajuba estuary (Fig. 2) (Supporting Information Data S1).

Dry bulk density varied from 0.41 to 0.77 g cm^{-3} in S1 (average 0.55 ± 0.11), from 0.43 to 0.61 g cm^{-3} in S2 (average 0.53 ± 0.06), from 0.53 to 0.83 g cm^{-3} in P1 (average 0.66 ± 0.08) and from 0.39 to 0.62 g cm^{-3} in P2 (average 0.52 ± 0.07) (Fig.2).

The ln^{210}Pb excess from all cores decreases with depth (Fig. 3), indicating minor sediment mixing during sedimentation. A constant sediment accretion rates was calculated to be 1.9 mm yr^{-1} for S1 ($r^2 = 0.73$; $n = 10$), 2.3 mm yr^{-1} for S2 ($r^2 = 0.76$; $n = 10$), 2.3 mm yr^{-1} for P1 ($r^2 = 0.65$; $n = 8$) and 3.1 mm yr^{-1} for P2 ($r^2 = 0.54$; $n = 11$) (Fig. 3). Age calculations based on these data indicate a c.125-yr record (1894–2019 C.E.), although some samples are beyond the range that can be dated reliably by the ^{210}Pb technique.

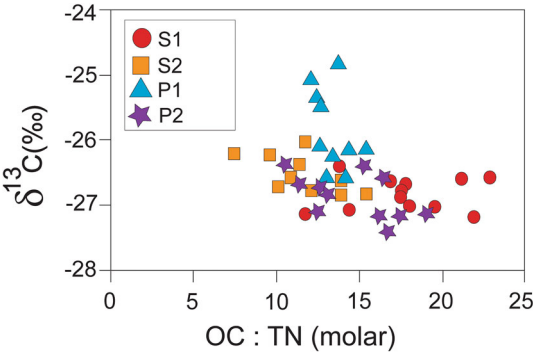

Fig. 5. Relationship between isotopic ($\delta^{13}C$) and OC : TN ratios in sediment cores of the Pará estuarine system in this study.

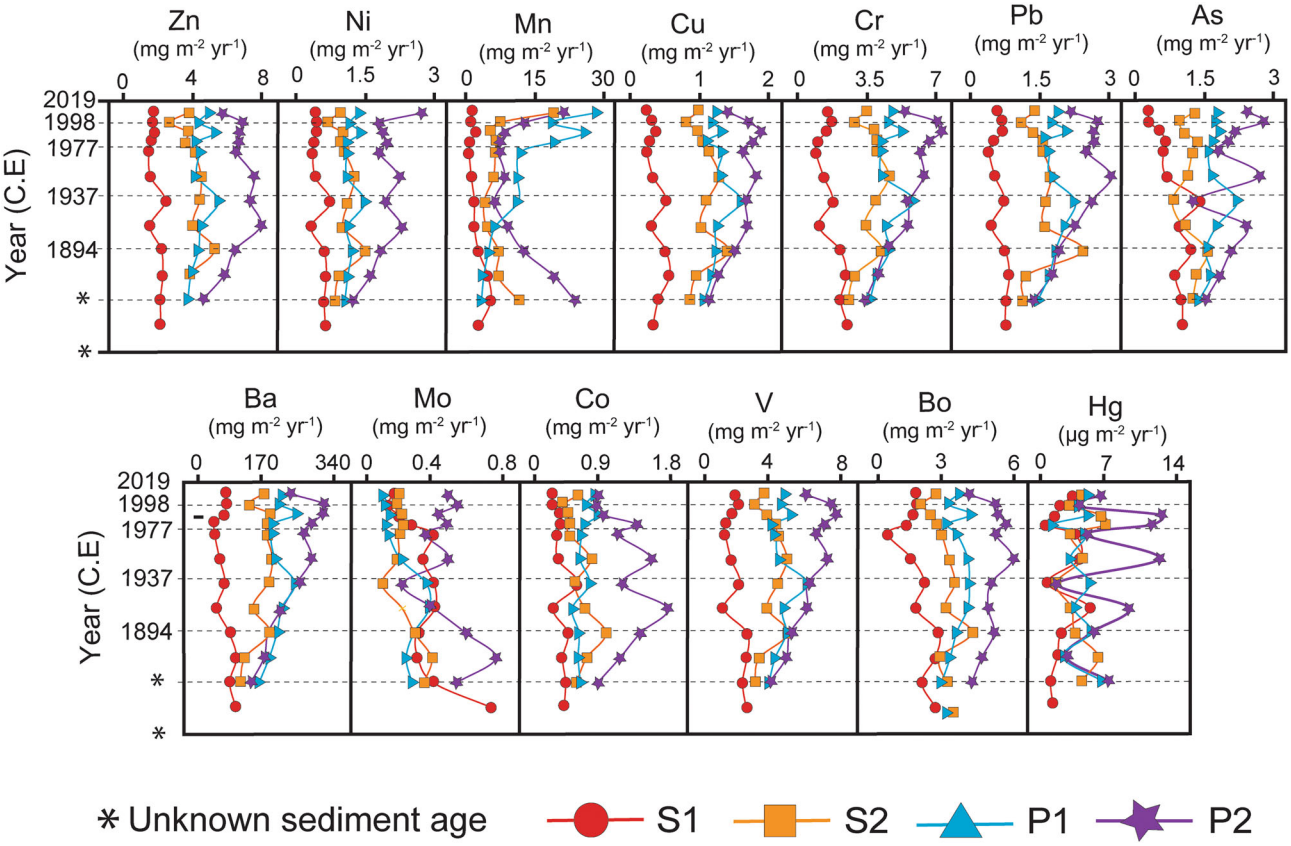

Fig. 6. Subsurface down core sediment trace metal accumulation for S1, S2, P1, and P2. *X*-axis show the content variation and *Y*-axis show year (C.E).

Carbon, nitrogen, phosphorus, and sulfur accumulation

No clear trends in carbon accumulation rates were observed in S2 and P1, while S1 and P2 show higher amplitude variation (Fig. 4). S1, S2, and P1 show an increase in carbon accumulation since the end of the 1990s. In contrast, P2 shows a significant decrease in organic carbon flux from c. 1997 to c. 2019, relative to from the period c. 1894 to c. 1977 (Table 1). The mean value recorded for S1 and S2 are 33.6 ± 6 and 29 ± 2.4 g m^{-2} yr^{-1}, respectively, while for P1 and P2 are 30.1 ± 5 and 59 ± 8.3 g m^{-2} yr^{-1}, respectively.

There is a trend in all cores toward higher nitrogen accumulation rates as depth decreases, with a reversal in all cores in the late 20th century, except for P1 (Fig. 4). Phosphorus accumulation rates were stable in S1 throughout the 125 yr record, but S2, P1, and P2 show a clear increasing trend from the end of the 1890s until the end of the 1990s, when a slight decrease is observed. Sulfur accumulation rates show a decrease upward in the S1 and P2 over the last 125 yr, and since 1998 for S2 and P1 (Fig. 4).

The $\delta^{13}C$ results in S1, S2, P1 and P2 varied from −27.45 to −24.77‰ (Table 1), and they all show an increasing trend from 1977 to 2019 (Fig. 4b). P1 shows higher values of $\delta^{13}C$ in the most recent periods, increasing particularly from 1977. $\delta^{15}N$ values varied from 2.37 to 4.87‰, and no clear trends are observed in general. C : N ratios varied from 7.58 to 22.92 (average 14.51 ± 3.32). There is a decreasing trend in C : N ratios throughout the record, shifting toward higher values from 1977 to 2019. The C : S ratios show an increasing trend upward in all cores, mostly since 1936 (Fig. 4).

Most of the organic matter is from terrestrial sources, mostly from C_3 vascular plants (e.g., mangrove plants). The most recent sediment increases both $\delta^{13}C$ and C : N ratios from 1977. In general, most of the results of $\delta^{13}C$ plotted against C : N ratios are in the same range, with exception of some results from recent sediments from P1 that show higher values of $\delta^{13}C$ and recent sediments from S1 that shows higher C : N molar ratios (Fig. 5).

Trace metal accumulation rates and enrichment factors

S1 results show trace metal accumulation rates lower than the other three cores for most of the elements analyzed (Fig. 6), except for Mo and Hg (*see* Supporting Information Data S2). The historical records of trace metals show stabilization and small shifts in accumulation over the last 125 yr in S1 for most of the elements analyzed, except for Hg and Bo, and Mo that shows a modest decrease in the most recent sediments.

In general, S2 and P1 show similar trends over the last c. 125 yr (Fig. 6), although differences in As around 1930s were observed. In addition, variations with similar patterns (increasing in P1 and decreasing in S2) were observed in accumulation in Pb, Cr, Bo, and Ba.

P2 shows the highest accumulation rates in this study, particularly in the most recent periods. A recurrent pattern of increasing historical accumulation with a modest decrease in the last three decades was observed in As, Pb, Cr, Cu, Zn, Bo, V, Co, and Ba. Hg, Mn, Mo, and Co presented the higher historical variations (Fig. 6). There was a sharp decrease in total sulfur content from the base toward the most recent sediments in all cores.

S2 and P2 have enrichment factors results < 1.5. P1 shows enrichment factors for Mn > 1.5, with a maximum of 3.7. S1 shows enrichment factors for As, Cu, and Hg > 1.5, with maximum values of 1.6, 1.7, and 4.5, respectively.

Discussion

Sedimentary characteristics and sediment accretion rates

Grain-size analysis is important as there is a direct relationship between mineral size and the capacity to sorb carbon, nutrient, and trace metals (Passos et al. 2021*b*). The mineral grain-size distribution of intertidal zones, including mangrove forests, is ultimately controlled by sources of sediment (Woodroffe et al. 1985) and hydrodynamic processes. The unique structures of mangrove forests act by reducing water velocity which enables suspended sediment settling (Mcleod et al. 2011; Passos et al. 2021*b*).

There was a relatively small historical grain-size variation at all sampled sites (Fig. 2), indicating a stable and consistent hydrodynamic in the last 125 yr. However, the southern part of the study in the Mocajuba estuary (P1 and P2) shows less variation and higher clay + silt content compared to the northern regions in the Curuçá estuary (S1 and S2), which suggests lower hydrodynamic changes on pristine mangroves of the region when compared to areas closer to shrimp farms, which was affected by the construction of shrimp ponds during the last 40 yr. Estuaries studied in the region are typically dominated by silt (Cohen and Lara 2003; Matos et al. 2020).

Sediment dry bulk density in blue carbon systems is important as it directly affects mass accumulation rates. Our results suggest that changes in ediment dry bulk density are not directly related to the proximity of shrimp farms. Our sampled mangrove forests have lower sediment dry bulk density when compared to urbanized mangroves in Brazil (1.21 ± 0.22 g cm^{-3}) (Passos et al. 2021*a*). However, the sediment dry bulk density from the sampled Amazon mangroves are similar to estuarine mangrove forests in Brazil (Kauffman et al. 2018*a*; Matos et al. 2020; de Oliveira Gomes et al. 2021), suggesting that geomorphological processes and proximity to land use changes may influence local sediment density.

Sediment mixing due to bioturbation and water movement (e.g., tidal processes and currents) can directly affect sediment accretion rates and sediment dating, however, the ln^{210}Pb excess from all cores decreases consistently with depth (Fig. 3), indicating minor sediment mixing. Sediment accretion rates in this study ranged from 1.9 to 3.1 mm yr^{-1}, which are lower than the sediment accretion rates from subtidal sediments in an estuary in the region (13–18 mm yr^{-1}; Matos et al. 2020). Sediment accretion rates from mangroves in southeast Brazil are also highly variable, ranging from 6.1 to 18.6 mm yr^{-1} (Sanders et al. 2006; Bernardino et al. 2020), also supporting high spatial variability in sediment accretion in mangrove forests. Although our sediment accretion rates data is within the range of global averages of 2.8 ± 16.9 mm yr^{-1} (Breithaupt et al. 2012), they are still in the lower spectrum of global average accretion rates in mangrove forests, which can be related to macro-tidal processes affecting the sediment accretion rates.

Sources of organic matter

The sources of organic matter in Mocajuba and Curuçá estuaries are primarily from C_3 terrestrial plants, likely from autochthonous sources, as observed by the relationship between stable isotopic ($\delta^{13}C$) and C : N molar ratios (Fig. 5) (Lamb et al. 2006). Similar $\delta^{13}C$ and C : N relationships are also observed in tropical mangroves elsewhere (Bernardino et al. 2020; Pérez et al. 2020; Passos et al. 2021*b*), including the Marapanim estuary near this study site (Matos et al. 2020). Higher $\delta^{13}C$ and C : N trends in more recent sediment (Figs. 4, 5) is observed in one pristine site (P1) from the late 1990s, suggesting a higher contribution of marine allochthonous carbon.

Carbon and nutrient accumulation

Organic carbon accumulation rates from these eastern Amazon mangrove forests ranged from 29.1 ± 2.4 to 59.1 ± 8.3 g m^{-2} yr^{-1}, which is considerably lower than the global average for mangrove forests recently estimated at 194 g m^{-2} yr^{-1} by Wang et al. (2021) and at 138 g m^{-2} yr^{-1} by Breithaupt and Steinmuller (2022). Previous studies estimated an average global carbon accumulation at 170 g m^{-2} yr^{-1} (Pérez et al. 2018), 163 g m^{-2} yr^{-1} (Breithaupt et al. 2012), 226 g m^{-2} yr^{-1} (Mcleod et al. 2011), and 115 g m^{-2} yr^{-1} (Bouillon et al. 2008). The higher organic carbon accumulation values in P2 are likely associated with higher sediment accretion rates and dry bulk density (Figs. 2, 3), rather than a significant increase in the organic carbon content in the sediment (Table 1), indicating a relatively constant carbon content along the forests in this region.

Estuaries along the Amazon coast, including the Mocajuba and Curuçá macro-tidal estuaries, are reported to have a thicker sediment mixed layers (Song et al. 2022) that might enhance organic matter decomposition and reduce carbon storage in coastal sediments. Sediment mixed layers are controlled by a combination of tidal oscillations, waves, and coastal currents, forming sediment layers of ~ 0.5–2 m thick

on sea bottom, which are also frequently reoxidized (Aller and Blair 2006). Song et al. (2022) suggested that sites with sediment mixed layers > 60 cm likely have lower organic carbon accumulation rates (< 50 g m^{-2} yr^{-1}), which is consistent with the average organic carbon accumulation rates found in this study 38 ± 13.5 g m^{-2} yr^{-1}. The combination of low dry bulk density, low sediment accretion rates and an oxic environment driven by sediment mixed layers process may explain low carbon accumulation on this study. In fact, the sedimentary C : S ratios supports oxidizing processes, showing lower values (< 3.0) in older sediments in all cores (Fig. 4), characteristics of anoxic sedimentary environments (Woolfe et al. 1995), and increasing sharply to oxic conditions (C : S > 10) toward the most recent sediments. The limited organic carbon accumulation at this region mirrors the low average carbon stocks in soils of this region (340 Mg C ha^{-1}; Kauffman et al. 2018*a*,*b*); which are nearly half of the global average (856 Mg C ha^{-1}; Kauffman et al. 2020).

Breithaupt et al. (2014) estimated global mangrove total nitrogen accumulation rates to be 8.9 ± 4.6 and 0.5 ± 0.5 g m^{-2} yr^{-1} for total phosphorus; but these rates are extremely variable globally. In Brazil, Passos et al. (2021*b*) determined an accumulation rate of 4.1 ± 2.1 g m^{-2} yr^{-1} for total nitrogen and 3.6 ± 2.3 g m^{-2} yr^{-1} for total phosphorus in a tropical mangrove forest in northeast Brazil, while Matos et al. (2020) reported an accumulation rate of 15.3 ± 4.1 g m^{-2} yr^{-1} for total nitrogen and 3.2 ± 0.8 g m^{-2} yr^{-1} for total phosphorus in a tidal creek ~ 25 km to the east of this study. The results in this study indicate an average of 2.7 ± 0.9 g m^{-2} yr^{-1} for total nitrogen and 4.3 ± 1.9 g m^{-2} yr^{-1} for total phosphorus. The total nitrogen accumulation rates in this study are lower than global averages (Bernardino et al. 2020), however, the total phosphorus accumulation seems to be considerably higher than global estimates (Breithaupt et al. 2014) and consistent with tropical mangroves elsewhere in Brazil (Matos et al. 2020; Passos et al. 2021*b*). The oxidation of nitrogen enhances nitrous oxide (N_2O) emissions, which may explain the low total nitrogen accumulation in this study. Conversely, the precipitation of P and Fe(III) oxyhydroxides due to oxidation via nitrate reduction may lead to a high retention of P in siliciclastic sediments (Lake et al. 2007).

Historical total phosphorus accumulation in S1 is lower than S2, P1, and P2, showing smaller variation throughout the 20th century until 2019 (Fig. 4). Conversely, S1 shows large shifts and a sharp increase in C : N ratios in recent sediments from 1998 (Fig. 4). This negative correlation between total phosphorus and C : N ratios could be related to shrimp ponds fertilizers being consumed during the autochthonous production of organic matter, as mangrove forests are efficient in sequestering nutrients from those type of activities (Passos et al. 2021*b*). S2, P1, and P2 show a large accumulation of total phosphorus and an increasing trend from the beginning of the 20th century. Historical increase of total phosphorus accumulation is an environmental parameter often used as evidence of anthropogenic impact related to specific types of development (e.g., agriculture) (Borges et al. 2009; Sanders et al. 2014; Passos et al. 2022).

Trace metal accumulation and enrichment factors

Trace metal content is often used to assess anthropogenic impact on mangrove ecosystems (Xavier et al. 2017; Passos et al. 2021*b*) and the environmental health of estuarine systems (Birch and Olmos 2008). Although numerous studies estimate the content of trace metals sorbed in surface sediments, there are few studies that reveal patterns of historical accumulation (mg m^{-2} yr^{-1}) in tropical mangrove ecosystems. Metal concentrations are sensitive to grain size, as metals are preferentially sorbed to clays and organic matter due to their high specific surface area (Vane et al. 2020).

This study shows small grain-size variations, except for S1 that has an increase in silt content at ~ 10–15 cm depth. This increase does not directly reflect an increase in metal content, which indicates that variations in trace metal concentrations are, in this case, decoupled by grain-size variations. Generally, the trace metal accumulation rates have a similar trend (Fig. 6), and no significant difference is observed between the samples collected near shrimp ponds sites (S1 and S2) and the pristine sites (P1 and P2). P2 shows a slightly higher accumulation rate due to higher sediment accretion rates (Fig. 2) and dry bulk density (Fig. 3) values. We argue that low trace accumulation rates in this study compared to other tropical mangroves impacted by aquaculture such as in India (Passos et al. 2022), China (Wu et al. 2017), and Brazil (Passos et al. 2021*b*) may be related to sediment mixed layers processes that might affect the capacity of sediment to adsorb trace metals dissolved in the water.

The trace metal dynamic in estuarine environments is affected by redox-sensitive processes and, thus, subjected to constant changes (Du Laing et al. 2009). For instance, Cu, Zn, Pb, and Ni, which are trace metals often used as a proxy for environmental contamination (Birch 2018), increase their solubility under oxic conditions (Gambrell et al. 1991). It is implying that some of the trace metals bound to minerals could be dissolved and leached during sediment mixed layers processes under oxic conditions, explaining lower accumulation near the shrimp ponds compared to mangrove forests elsewhere (Passos et al. 2022).

Enrichment factors are widely used to assess the magnitude of anthropogenic impact in estuarine environments (Xavier et al. 2017), where enrichment factors > 1.5 is considered as evidence of anthropogenic impact (Conrad et al. 2017). The enrichment factor for Hg, As and Cu was found to be 4.5, 1.6, and 1.7, respectively, in the shrimp pounds site, while Mn was found to be 3.7 on the site distant from the shrimp pounds. Hg was found to be the highest enrichment factor, up to 4.5-fold higher than the base lines values (Table 2). The accumulation of sulfides, common in mangrove sediments, may cause precipitation on inorganic Hg in a highly insoluble

Table 2. Minimum and maximum values for trace metals enrichment factors (EF) for S1, S2, P1, and P2.

	EF S1		EF S2		EF P1		EF P2	
Element	Min	Max	Min	Max	Min	Max	Min	Max
As	0.5	1.6	0.5	1.0	0.9	1.1	0.6	1.0
Pb	1.0	1.4	0.8	1.2	0.9	1.1	0.9	1.1
Cr	0.9	1.0	1.0	1.0	1.0	1.1	0.9	1.0
Cu	1.0	1.7	0.8	1.0	0.9	1.1	0.7	1.0
Mn	0.9	1.4	0.3	1.2	1.0	3.7	0.2	1.0
Ni	1.0	1.4	0.8	1.0	0.9	1.0	0.7	1.3
Zn	1.0	1.5	0.8	1.0	0.9	1.1	0.7	1.0
Hg	0.9	4.5	0.3	1.2	0.3	1.0	0.2	1.0
Bo	0.7	1.3	0.6	1.0	0.9	1.2	0.6	1.0
V	1.0	1.2	0.8	1.0	1.0	1.0	0.9	1.0
Co	0.9	1.7	0.6	1.1	0.7	1.0	0.5	1.2
Mo	0.3	1.1	0.3	1.0	0.4	1.1	0.3	1.1
Ba	0.9	1.1	1.0	1.1	1.0	1.1	0.9	1.1

HgS mineral (cinnabar) (Kaplan et al. 2002), which may explain higher Hg accumulation compared to the other trace metals in this study. This high enrichment factors for Hg can be associated with anthropogenic activities such as mining and fertilizers for aquaculture, as observed elsewhere (Machado et al. 2016). If the Hg is not sorbed in the minerals and organic matter, and exported from the estuary, it can be available as methylmercury via microbial processes and lead to ecotoxicity through bioaccumulation in the marine food web (Kehrig et al. 2010). Manganese enrichment factor values can also be associated to mining and fertilizers for agriculture/aquaculture (Li et al. 2014), and studies indicate that high values can cause health issues in humans (Batterman et al. 2011) and plants (Paschke et al. 2005). Arsenic and Cu have enrichment factors slightly above the evidence of anthropogenic impact. For As, similar enrichment values were also observed on sites of the Brazilian coast and associated to natural geogenic sources from the Barreiras Formation and postdepositional diagenetic processes (Barcellos et al. 2017; Xavier et al. 2017). Mercury and Mn high enrichment factor values found on this study could be a consequence of local mining activities and the use of fertilizer for aquaculture/agriculture, as observed in wetland sediments elsewhere (Liang et al. 2015; Passos et al. 2021*b*). The other trace metals that show enrichment factors < 1.5 are likely derived from geogenic processes or atmospheric deposition on the catchment (Barcellos et al. 2017).

Conclusions

Here, we provide empirical evidence for the sequestration of carbon, nutrients and trace metals in a macro-tidal mangrove forest in the Amazon coast over more than a century. Our study revealed historical and spatial variability in accumulation rates in Amazon mangrove forests in close proximity and under contrasting land use scenarios, revealing a marked variability in carbon sequestration rates. Organic carbon accumulation rates are fivefold lower than global averages for mangrove forests. Trace metals accumulation rates are also limited compared to other tropical mangrove forests elsewhere, but high enrichment factors may indicate an increasing human footprint on the coastal Amazon. We suggest that the low rates of carbon accumulation in these eastern Amazon mangroves are associated with sediment mixed layer processes driving oxidation of recent buried carbon. We constrain carbon accumulation in a highly dynamic macro-tidal tropical estuary, but advise caution with extrapolations based on limited spatial sampling to constrain nation-wide estimates of carbon sequestration. Resolving this regional variability in mangrove carbon burial should be prioritized in Brazil, particularly in the current scenario of climate change mitigation strategies for reducing CO_2 emissions and the implementation carbon offset schemes initiatives.

Data availability statement

Data supporting the findings of this study are available within article, and in the Supporting Information, and raw data are available on request from the authors.

References

Aller, R. C., and N. E. Blair. 2006. Carbon remineralization in the Amazon–Guianas tropical mobile mudbelt: A sedimentary incinerator. Cont. Shelf Res. **26**: 2241–2259. doi:10.1016/j.csr.2006.07.016

Alongi, D. M. 2014. Carbon cycling and storage in mangrove forests. Ann. Rev. Mar. Sci. **6**: 195–219. doi:10.1146/annurev-marine-010213-135020

Appleby, P., and F. Oldfield. 1992. Application of ^{210}Pb to sedimentation studies, p. 731–778. *In* M. Ivanovich and R. S. Harmon [eds.], Uranium-series disequilibrium: Application to earth. Marine, and environmental sciences. Clarendon Press.

Barcellos, R. L., R. C. L. Figueira, E. J. Franç, C. A. Schettini, and D. De Arruda Xavier. 2017. Changes of estuarine sedimentation patterns by urban expansion: The case of middle Capibaribe Estuary, northeastern Brazil. Int. J. Geosci. **8**: 514–535. doi:10.4236/ijg.2017.84027

Batterman, S., F.-C. Su, C. Jia, R. N. Naidoo, T. Robins, and I. Naik. 2011. Manganese and lead in children's blood and airborne particulate matter in Durban, South Africa. Sci. Total Environ. **409**: 1058–1068. doi:10.1016/j.scitotenv.2010.12.017

Bernardino, A. F., S. A. Netto, P. R. Pagliosa, F. Barros, R. A. Christofoletti, J. S. Rosa Filho, A. Colling, and P. C. Lana. 2015. Predicting ecological changes on benthic estuarine assemblages through decadal climate trends along Brazilian

marine ecoregions. Estuar. Coast. Shelf Sci. **166**: 74–82. doi:10.1016/j.ecss.2015.05.021

Bernardino, A. F., C. J. Sanders, L. B. Bissoli, L. E. D. O. Gomes, J. B. Kauffman, and T. O. Ferreira. 2020. Land use impacts on benthic bioturbation potential and carbon burial in Brazilian mangrove ecosystems. Limnol. Oceanogr. **65**: 2366–2376. doi:10.1002/lno.11458

Bernardino, A. F., G. N. Nóbrega, and T. O. Ferreira. 2021. Consequences of terminating mangrove's protection in Brazil. Mar. Policy **125**: 104389. doi:10.1016/j.marpol.2020.104389

Bernardino, A. F., and others. 2022. The novel mangrove environment and composition of the Amazon Delta. Curr. Biol. **32**: 3636–3640.e2. doi:10.1016/j.cub.2022.06.071

Birch, G. 2018. A review of chemical-based sediment quality assessment methodologies for the marine environment. Mar. Pollut. Bull. **133**: 218–232. doi:10.1016/j.marpolbul.2018.05.039

Birch, G. F., and M. A. Olmos. 2008. Sediment-bound heavy metals as indicators of human influence and biological risk in coastal water bodies. ICES J. Mar. Sci. **65**: 1407–1413. doi:10.1093/icesjms/fsn139

Borges, A., C. Sanders, H. Santos, D. Araripe, W. Machado, and S. Patchineelam. 2009. Eutrophication history of Guanabara Bay (SE Brazil) recorded by phosphorus flux to sediments from a degraded mangrove area. Mar. Pollut. Bull. **58**: 1750–1754. doi:10.1016/j.marpolbul.2009.07.025

Bouillon, S., and others. 2008. Mangrove production and carbon sinks: A revision of global budget estimates. Glob. Biogeochem. Cycles **22**. doi:10.1029/2007GB003052

Breithaupt, J. L., and H. E. Steinmuller. 2022. Refining the global estimate of mangrove carbon burial rates using sedimentary and geomorphic settings. Geophys. Res. Lett. **49**: e2022GL100177. doi:10.1029/2022GL100177

Breithaupt, J. L., J. M. Smoak, T. J. Smith, C. J. Sanders, and A. Hoare. 2012. Organic carbon burial rates in mangrove sediments: Strengthening the global budget. Glob. Biogeochem. Cycles **26**. doi:10.1029/2012GB004375

Breithaupt, J. L., J. M. Smoak, T. J. Smith III, and C. J. Sanders. 2014. Temporal variability of carbon and nutrient burial, sediment accretion, and mass accumulation over the past century in a carbonate platform mangrove forest of the Florida Everglades. J. Geophys. Res.: Biogeosciences **119**: 2032–2048. doi:10.1002/2014JG002715

Cohen, M. C., and R. J. Lara. 2003. Temporal changes of mangrove vegetation boundaries in Amazonia: Application of GIS and remote sensing techniques. Wetl. Ecol. Manag. **11**: 223–231. doi:10.1023/A:1025007331075

Conrad, S. R., I. R. Santos, D. R. Brown, L. M. Sanders, M. L. van Santen, and C. J. Sanders. 2017. Mangrove sediments reveal records of development during the previous century (Coffs Creek estuary, Australia). Mar. Pollut. Bull. **122**: 441–445. doi:10.1016/j.marpolbul.2017.05.052

Cutshall, N. H., I. L. Larsen, and C. R. Olsen. 1983. Direct analysis of ^{210}Pb in sediment samples: Self-absorption corrections. Nucl. Instrum. Methods Phys. Res. **206**: 309–312. doi:10.1016/0167-5087(83)91273-5

de Oliveira Gomes, L. E., C. J. Sanders, G. N. Nobrega, L. C. Vescovi, H. M. Queiroz, J. B. Kauffman, T. O. Ferreira, and A. F. Bernardino. 2021. Ecosystem carbon losses following a climate-induced mangrove mortality in Brazil. J. Environ. Manage. **297**: 113381. doi:10.1016/j.jenvman.2021.113381

Du Laing, G., J. Rinklebe, B. Vandecasteele, E. Meers, and F. M. Tack. 2009. Trace metal behaviour in estuarine and riverine floodplain soils and sediments: A review. Sci. Total Environ. **407**: 3972–3985. doi:10.1016/j.scitotenv.2008.07.025

Gambrell, R., J. Wiesepape, W. Patrick, and M. Duff. 1991. The effects of pH, redox, and salinity on metal release from a contaminated sediment. Water Air Soil Pollut. **57**: 359–367. doi:10.1007/BF00282899

Gomes, V. J., N. E. Asp, E. Siegle, J. D. Gomes, A. M. Silva, A. S. Ogston, and C. A. Nittrouer. 2021. Suspended-sediment distribution patterns in tide-dominated estuaries on the eastern amazon coast: Geomorphic controls of turbidity-maxima formation. Water **13**: 1568. doi:10.3390/w13111568

Kaplan, D., A. Knox, and J. Myers. 2002. Mercury geochemistry in wetland and its implications for in situ remediation. J. Environ. Eng. **128**: 723–732. doi:10.1061/(ASCE)0733-9372(2002)128:8(723)

Kauffman, J. B., A. F. Bernardino, T. O. Ferreira, N. W. Bolton, L. E. D. O. Gomes, and G. N. Nobrega. 2018*a*. Shrimp ponds lead to massive loss of soil carbon and greenhouse gas emissions in northeastern Brazilian mangroves. Ecol. Evol. **8**: 5530–5540. doi:10.1002/ece3.4079

Kauffman, J. B., A. F. Bernardino, T. O. Ferreira, L. R. Giovannoni, L. E. de O Gomes, D. J. Romero, L. C. Z. Jimenez, and F. Ruiz. 2018*b*. Carbon stocks of mangroves and salt marshes of the Amazon region, Brazil. Biol. Lett. **14**: 20180208. doi:10.1098/rsbl.2018.0208

Kauffman, J. B., and others. 2020. Total ecosystem carbon stocks of mangroves across broad global environmental and physical gradients. Ecol. Monogr. **90**: e01405. doi:10.1002/ecm.1405

Kehrig, H. A., T. G. Seixas, A. P. Baêta, O. Malm, and I. Moreira. 2010. Inorganic and methylmercury: Do they transfer along a tropical coastal food web? Mar. Pollut. Bull. **60**: 2350–2356. doi:10.1016/j.marpolbul.2010.08.010

Kristensen, E., S. Bouillon, T. Dittmar, and C. Marchand. 2008. Organic carbon dynamics in mangrove ecosystems: A review. Aquat. Bot. **89**: 201–219. doi:10.1016/j.aquabot.2007.12.005

Lake, B. A., K. M. Coolidge, S. A. Norton, and A. Amirbahman. 2007. Factors contributing to the internal loading of phosphorus from anoxic sediments in six Maine, USA, lakes. Sci.

Total Environ. **373**: 534–541. doi:10.1016/j.scitotenv.2006.12.021

Lamb, A. L., G. P. Wilson, and M. J. Leng. 2006. A review of coastal palaeoclimate and relative sea-level reconstructions using $\delta^{13}C$ and C/N ratios in organic material. Earth-Sci. Rev. **75**: 29–57. doi:10.1016/j.earscirev.2005.10.003

Li, P., H. Qian, K. W. Howard, J. Wu, and X. Lyu. 2014. Anthropogenic pollution and variability of manganese in alluvial sediments of the Yellow River, Ningxia, Northwest China. Environ. Monit. Assess. **186**: 1385–1398. doi:10.1007/s10661-013-3461-3

Liang, J., and others. 2015. Spatial and temporal variation of heavy metal risk and source in sediments of Dongting Lake wetland, mid-South China. J. Environ. Sci. Health A Tox. Hazard. Subst. Environ. Eng. **50**: 100–108. doi:10.1080/10934529.2015.964636

Lovelock, C. E., M. F. Adame, V. Bennion, M. Hayes, J. O'Mara, R. Reef, and N. S. Santini. 2014. Contemporary rates of carbon sequestration through vertical accretion of sediments in mangrove forests and saltmarshes of south East Queensland, Australia. Estuaries Coasts **37**: 763–771. doi:10.1007/s12237-013-9702-4

Lovelock, C. E., and others. 2015. The vulnerability of indo-Pacific mangrove forests to sea-level rise. Nature **526**: 559–563. doi:10.1038/nature15538

Machado, W., C. J. Sanders, I. R. Santos, L. M. Sanders, E. V. Silva-Filho, and W. Luiz-Silva. 2016. Mercury dilution by autochthonous organic matter in a fertilized mangrove wetland. Environ. Pollut. **213**: 30–35. doi:10.1016/j.envpol.2016.02.002

Macreadie, P. I., K. Allen, B. P. Kelaher, P. J. Ralph, and C. G. Skilbeck. 2012. Paleoreconstruction of estuarine sediments reveal human-induced weakening of coastal carbon sinks. Glob. Change Biol. **18**: 891–901. doi:10.1111/j.1365-2486.2011.02582.x

Macreadie, P. I., and others. 2019. The future of blue carbon science. Nat. Commun. **10**: 3998. doi:10.1038/s41467-019-11693-w

Matos, C. R., J. F. Berrêdo, W. Machado, C. J. Sanders, E. Metzger, and M. C. Cohen. 2020. Carbon and nutrients accumulation in tropical mangrove creeks, Amazon region. Mar. Geol. **429**: 106317. doi:10.1016/j.margeo.2020.106317

Mcleod, E., and others. 2011. A blueprint for blue carbon: Toward an improved understanding of the role of vegetated coastal habitats in sequestering CO2. Front. Ecol. Environ. **9**: 552–560. doi:10.1890/110004

Miola, B., J. O. de Morais, and L. de Souza Pinheiro. 2016. Trace metal concentrations in tropical mangrove sediments, NE Brazil. Mar. Pollut. Bull. **102**: 206–209. doi:10.1016/j.marpolbul.2015.11.039

Moore, W. S. 1984. Radium isotope measurements using germanium detectors. Nucl. Instrum. Methods Phys. Res. **223**: 407–411. doi:10.1016/0167-5087(84)90683-5

Mourão, F. V., and others. 2020. Water quality and eutrophication in the Curuçá estuary in northern Brazil. Reg. Stud. Mar. Sci. **39**: 101450. doi:10.1016/j.rsma.2020.101450

Naidu, A., L. Cooper, B. Finney, R. Macdonald, C. Alexander, and I. P. Semiletov. 2000. Organic carbon isotope ratios ($\delta^{13}C$) of Arctic Amerasian continental shelf sediments. Int. J. Earth Sci. **89**: 522–532. doi:10.1007/s005310000121

Nóbrega, G., T. Ferreira, R. Romero, A. Marques, and X. Otero. 2013. Iron and sulfur geochemistry in semi-arid mangrove soils (Ceará, Brazil) in relation to seasonal changes and shrimp farming effluents. Environ. Monit. Assess. **185**: 7393–7407. doi:10.1007/s10661-013-3108-4

Nóbrega, G. N., T. O. Ferreira, M. S. Neto, H. M. Queiroz, A. G. Artur, E. D. S. Mendonça, E. D. O. Silva, and X. L. Otero. 2016. Edaphic factors controlling summer (rainy season) greenhouse gas emissions (CO_2 and CH_4) from semiarid mangrove soils (NE-Brazil). Sci. Total Environ. **542**: 685–693. doi:10.1016/j.scitotenv.2015.10.108

Nóbrega, G. N., T. O. Ferreira, M. Siqueira Neto, E. D. S. Mendonça, R. E. Romero, and X. L. Otero. 2019. The importance of blue carbon soil stocks in tropical semiarid mangroves: A case study in northeastern Brazil. Environ. Earth Sci. **78**: 369. doi:10.1007/s12665-019-8368-z

Paschke, M. W., A. Valdecantos, and E. F. Redente. 2005. Manganese toxicity thresholds for restoration grass species. Environ. Pollut. **135**: 313–322. doi:10.1016/j.envpol.2004.08.006

Passos, T., D. Penny, C. Sanders, E. De França, T. Oliveira, L. Santos, and R. Barcellos. 2021*a*. Mangrove carbon and nutrient accumulation shifts driven by rapid development in a tropical estuarine system, northeast Brazil. Mar. Pollut. Bull. **166**: 112219. doi:10.1016/j.marpolbul.2021.112219

Passos, T., C. J. Sanders, R. Barcellos, and D. Penny. 2021*b*. Assessment of the temporal retention of mercury and nutrient records within the mangrove sediments of a highly impacted estuary. Environ. Res. **206**: 112569. doi:10.1016/j.envres.2021.112569

Passos, T., D. Penny, R. Barcellos, S. B. Nandan, D. S. Babu, I. R. Santos, and C. J. Sanders. 2022. Increasing carbon, nutrient and trace metal accumulation driven by development in a mangrove estuary in South Asia. Sci. Total Environ. **832**: 154900. doi:10.1016/j.scitotenv.2022.154900

Pérez, A., W. Machado, D. Gutiérrez, A. Borges, S. Patchineelam, and C. J. Sanders. 2018. Carbon accumulation and storage capacity in mangrove sediments three decades after deforestation within a eutrophic bay. Mar. Pollut. Bull. **126**: 275–280. doi:10.1016/j.marpolbul.2017.11.018

Pérez, A., W. Machado, D. Gutiérrez, M. S. Saldarriaga, and C. J. Sanders. 2020. Shrimp farming influence on carbon and nutrient accumulation within Peruvian mangroves sediments. Estuar. Coast. Shelf Sci. **243**: 106879. doi:10.1016/j.ecss.2020.106879

Ravichandran, M., M. Baskaran, P. H. Santschi, and T. S. Bianchi. 1995. Geochronology of sediments in the Sabine-

Neches estuary, Texas, USA. Chem. Geol. **125**: 291–306. doi:10.1016/0009-2541(95)00082-W

Rogers, K., and others. 2019. Wetland carbon storage controlled by millennial-scale variation in relative sea-level rise. Nature **567**: 91–95. doi:10.1038/s41586-019-0951-7

Rossetti, D. F., F. H. Bezerra, and J. M. Dominguez. 2013. Late Oligocene–Miocene transgressions along the equatorial and eastern margins of Brazil. Earth-Sci. Rev. **123**: 87–112. doi:10.1016/j.earscirev.2013.04.005

Sanders, C. J., I. R. Santos, E. V. Silva-filho, and S. R. Patchineelam. 2006. Mercury flux to estuarine sediments, derived from Pb-210 and Cs-137 geochronologies (Guaratuba Bay, Brazil). Mar. Pollut. Bull. **52**: 1085–1089. doi:10.1016/j.marpolbul.2006.06.004

Sanders, C. J., J. M. Smoak, A. S. Naidu, L. M. Sanders, and S. R. Patchineelam. 2010. Organic carbon burial in a mangrove forest, margin and intertidal mud flat. Estuar. Coast. Shelf Sci. **90**: 168–172. doi:10.1016/j.ecss.2010.08.013

Sanders, C. J., and others. 2014. Elevated rates of organic carbon, nitrogen, and phosphorus accumulation in a highly impacted mangrove wetland. Geophys. Res. Lett. **41**: 2475–2480. doi:10.1002/2014GL059789

Sanders, C. J., and others. 2016. Examining $^{239+240}$Pu, ^{210}Pb and historical events to determine carbon, nitrogen and phosphorus burial in mangrove sediments of Moreton Bay, Australia. J. Environ. Radioact. **151**: 623–629. doi:10.1016/j.jenvrad.2015.04.018

Sippo, J. Z., and others. 2020. Coastal carbon cycle changes following mangrove loss. Limnol. Oceanogr. **65**: 2642–2656. doi:10.1002/lno.11476

Song, S., and others. 2022. A global assessment of the mixed layer in coastal sediments and implications for carbon storage. Nat. Commun. **13**: 4903. doi:10.1038/s41467-022-32650-0

Sperazza, M., J. N. Moore, and M. S. Hendrix. 2004. High-resolution particle size analysis of naturally occurring very fine-grained sediment through laser diffractometry. J. Sediment. Res. **74**: 736–743. doi:10.1306/031104740736

Vane, C. H., A. W. Kim, J. F. Emmings, G. H. Turner, V. Moss-Hayes, J. A. Lort, and P. J. Williams. 2020. Grain size and organic carbon controls polyaromatic hydrocarbons (PAH), mercury (Hg) and toxicity of surface sediments in the river Conwy Estuary, Wales, UK. Mar. Pollut. Bull. **158**: 111412. doi:10.1016/j.marpolbul.2020.111412

Wang, F., and others. 2021. Global blue carbon accumulation in tidal wetlands increases with climate change. Natl. Sci. Rev. **8**: nwaa296. doi:10.1093/nsr/nwaa296

Woodroffe, C. D., B. G. Thom, and J. Chappell. 1985. Development of widespread mangrove swamps in mid-Holocene times in northern Australia. Nature **317**: 711–713. doi:10.1038/317711a0

Woolfe, K. J., P. J. Dale, and G. J. Brunskill. 1995. Sedimentary C/S relationships in a large tropical estuary: Evidence for refractory carbon inputs from mangroves. Geo-Mar. Lett. **15**: 140–144. doi:10.1007/BF01204455

Wu, H., and others. 2017. Trace metals in sediments and benthic animals from aquaculture ponds near a mangrove wetland in southern China. Mar. Pollut. Bull. **117**: 486–491. doi:10.1016/j.marpolbul.2017.01.026

Xavier, D. D. A., C. A. Schettini, R. C. Figueira, and R. L. Barcellos. 2017. Determination of geochemical background values on a tropical estuarine system in a densely urban area. Case study: Capibaribe estuary, northeastern Brazil. Mar. Pollut. Bull. **123**: 381–386. doi:10.1016/j.marpolbul.2017.09.007

Zhang, J., and C. Liu. 2002. Riverine composition and estuarine geochemistry of particulate metals in China—Weathering features, anthropogenic impact and chemical fluxes. Estuar. Coast. Shelf Sci. **54**: 1051–1070. doi:10.1006/ecss.2001.0879

Acknowledgments

Tiago Passos is funded by an Australia Government Research Training Program (RTP) scholarship. Laboratory investigations were made possible by the Australian Research Council (LE140100083). Field work was supported by the National Geographic Society grant NGS-50638R-18 to A.F.B. Gabriel N. Nóbrega is supported by FUNCAP research fellow (Chief Scientist Program for the Environment—Climate change mitigation and adaptation project). Open access publishing facilitated by The University of Sydney, as part of the Wiley - The University of Sydney agreement via the Council of Australian University Librarians.

Conflict of Interest

None declared.

Submitted 04 December 2022
Revised 02 May 2023
Accepted 15 June 2023

Associate editor: Anna R Armitage